

The MAX-DOAS network in Mexico City to measure atmospheric pollutants

JOSUÉ ARELLANO, ARNE KRÜGER, CLAUDIA RIVERA, WOLFGANG STREMME,

MARTINA M. FRIEDRICH, ALEJANDRO BEZANILLA and MICHEL GRUTTER

Centro de Ciencias de la Atmósfera, Universidad Nacional Autónoma de México, Circuito Exterior,

Ciudad Universitaria, 04510 Ciudad de México

Corresponding author: Michel Grutter; email: grutter@unam.mx

Received: November 5, 2015; accepted: March 9, 2016

RESUMEN

Se construyó un instrumento basado en la técnica de espectroscopía óptica de absorción diferencial con múltiples ejes (MAX-DOAS, por sus siglas en inglés) para medir luz esparcida en la región UV-visible en diferentes ángulos de elevación. De los espectros medidos se obtuvieron densidades de columna inclinada (SCD, por sus siglas en inglés) para gases específicos como el dióxido de nitrógeno (NO_2) y formaldehído (HCHO) que absorben en esta región. En esta contribución se presentan las características técnicas y el desempeño de los instrumentos, su despliegue en una nueva red de observaciones formada dentro de la zona metropolitana de la Ciudad de México, así como algunos resultados de SCD de los gases NO_2 y HCHO. Estas mediciones proporcionan una visión más clara sobre la distribución vertical, espacial y la variabilidad de contaminantes atmosféricos clave, que también sirven como base para los estudios de validación presentes y futuros de sensores satelitales.

ABSTRACT

An instrument based on the Multi Axis Differential Optical Absorption Spectroscopy (MAX-DOAS) technique was designed and constructed to measure scattered sunlight in the UV-visible region at different elevation angles. Slant column densities (SCDs) of specific gas absorbers such as nitrogen dioxide (NO_2) and formaldehyde (HCHO) are derived from the measured spectra. In this contribution, the technical characteristics and performance of the instruments, their deployment in a newly formed observational network within the metropolitan area of Mexico City, and some results of the retrieved NO_2 and HCHO SCDs are presented. These measurements provide more insight on the vertical and spatial distribution of these key atmospheric pollutants and their temporal variability, which also serve as a basis for present and future satellite validation studies.

Keywords: MAX-DOAS instrument, slant columns, nitrogen dioxide (NO_2), formaldehyde (HCHO), air pollution, Mexico City.

1. Introduction

Air pollution continues to be a relevant and continuously growing problem due to its impact on health, the ecosystems and climate. It is considered the world's largest single environmental health risk and according to the World Health Organization, in 2012 more than 3 million people died prematurely as a result of ambient air pollution exposure (WHO, 2014). The Mexico City Metropolitan Area (MCMA), located within a high altitude basin 2200 masl,

has over 21 million inhabitants (WPR, 2014) and although some improvements have been accomplished in recent years, there are still serious issues with the pollution levels. A recent emission inventory for 2012 reports that 5.5×10^{17} J of fuel were burned during that year from the transport (58.8%), industrial (25.2%), residential (13.4%) and commercial (2.6%) sectors. According to this report, the fuel consumption has been steadily growing during the last decades, particularly from the transport sector,

which now consists of more than 5 million vehicles burning mostly gasoline and natural gas (SEDEMA, 2013).

Nitrogen dioxide (NO_2), produced mainly from the combustion of fossil fuels, is an important air pollutant and a key contributor to photochemical smog. Almost 900 thousand tons of NO_x ($\text{NO} + \text{NO}_2$) were emitted during 2012 (SEDEMA, 2013). Surface NO_2 levels have continuously been monitored by the local government and data from Mexico City's automatic air quality monitoring network (Red Automática de Monitoreo Atmosférico, RAMA) is available since 1986 (starting with 10 stations). Currently the network has 29 active stations that are spread throughout the MCMA (<http://www.aire.df.gob.mx>). Formaldehyde (HCHO) is the most abundant carbonyl compound in the atmosphere; this substance, which comes from primary emissions as well as secondary photochemical production, has harmful carcinogenic properties (García *et al.*, 2006). HCHO levels, with average daily maxima ranging between 22 ppb in July–October to 28 ppb in March–May, have been measured with long-path Fourier Transform Infrared Spectroscopy (FTIR) and Differential Optical Absorption Spectroscopy (DOAS) (Grutter *et al.*, 2005).

There have been some studies to evaluate the vertical column densities of NO_2 in Mexico City. Melamed *et al.* (2009) deployed a zenith scattered light DOAS south-east of Mexico City to characterize pollution transport events during the MILAGRO field campaign in 2006. Data from in situ and ceilometer measurements at particular events were analyzed in conjunction with meteorological data and characteristic transport patterns were identified. Also during MILAGRO on March 10, 2006 a ground-based traversal measurement from east to north-west of the city was carried out with two mobile zenith scattered light DOAS instruments, and a cross-section of the pollution plume could be detected (Johansson *et al.*, 2009). With these measurements the authors were able to estimate the outflow of both NO_2 and HCHO from the MCMA on that particular day and compare them with model results. Another study by Rivera *et al.* (2013) using fixed zenith scattered DOAS measurements within the MCMA, was used to determine the variability of the differential NO_2 columns. These were then compared with column amounts derived from surface and mixing layer heights (MLH) from a ceilometer, and those from satellite observations

produced by the Ozone Monitoring Instrument (OMI). The ground-based results, both from DOAS and in situ/MLH data, were considerably higher than the OMI column amounts.

Determining the vertical profile of a gas can be accomplished by performing in situ measurements from aircrafts, balloons or unmanned aerial vehicles. However, in order to observe the variability with enough time resolution and for longer time periods, remote sensing techniques are preferred. Active long-path DOAS measurements at different elevation angles using retro-reflectors installed at various heights have been done in order to gain information on the vertical distribution of the pollutants (Stutz *et al.*, 2002), however, the deployment of such an experimental set-up is complicated. MAX-DOAS is a passive technique which measures scattered sunlight at zenith and at different elevation angles, increasing the optical path and thus the sensitivity of the absorbing species (Hönniger *et al.*, 2004a; Platt and Stutz, 2008). Some information on the vertical distribution of the gases can be obtained with this technique by using a radiative transfer model and applying inversion methods on the retrieved SCD. Several MAX-DOAS instruments have been constructed and deployed providing valuable information of the vertical distribution of pollution (Carlson *et al.*, 2010; Coburn *et al.*, 2011; Hönniger *et al.*, 2004b; Hendrick *et al.*, 2014).

In this work, we present the technical characteristics of the MAX-DOAS instrument constructed at the National Autonomous University of Mexico (UNAM) as well as some results of the first retrieved SCDs at low elevation angles. Four instruments, installed within the MCMA to form a MAX-DOAS network in Mexico City, are fully automated allowing continuous daily operation throughout the year. A code has been developed based on radiative transfer and inversion models using the measurements from all the elevation angles in order to obtain more information on the vertical distribution and thus a better estimate of the vertical column densities (VCD's). The code and the results will be presented in a forthcoming paper.

2. Experimental

2.1 Instrumentation

We have designed and developed an instrument based on the Multi Axis Differential Optical Absorption Spectroscopy (MAX-DOAS) technique

in the Spectroscopy Lab of the Centro de Ciencias de la Atmósfera (Center for Atmospheric Sciences) at UNAM. This instrument can automatically and continuously measure the spectroscopically-resolved solar scattered radiation at different elevation angles. It is composed of the two main parts described below: the scanner and the acquisition/control units.

2.1.1 Scanner

The scanner collects, with a narrow field-of-view (FOV), atmospheric scattered solar radiation at different elevation angles and sends it to the acquisition/control unit for spectroscopic analysis. Figure 1 shows the parts that make up the scanner, which is installed in the open sky. Light is collected by a telescope (fig. 1b) constructed with a plano-convex quartz lens (Edmund Optics, $\varnothing = 25.4$ mm, $f = 100$ mm), mounted inside a hollow Nylamid cylinder (resistant to sunlight) custom manufactured to hold the lens and the optical fiber connector at the other end, at a depth corresponding to the focal length of the lens.

The telescope body has a motor-controlled shutter (Fig. 1b) installed close to where the optical fiber is connected. A 5 mm slot is cut across the Nylamid cylinder allowing the light path to be obstructed just before the optical fiber connector when the shutter plate is closed. The shutter, used for measurements of the dark spectra between scans, is mounted to the telescope body with a Nylamid ring and a fixing screw. It consists of a circular plate (50 mm in radius) which is rotated with an angle of 55° into the slot using a small stepper motor (Mercury, 7.5° per step). An optical switch is used to indicate the open position of the shutter plate.

The telescope is fixed and introduced into an enclosure (NEMA-rated type 3), so that only 10 mm of the telescope is out of the box. A 50.8 mm × 100 mm PVC pipe, painted in black, is placed around the telescope to keep it under shadow and for protection (fig. 1a). The scanner enclosure (200 × 200 × 120 mm) is resistant to sunlight, hermetically sealed to protect the inner parts from external conditions like rain, wind and bugs, and uses gland connectors for the cables (optical fiber and communication cable). These factors are important when operating the instruments during long periods and in harsh weather conditions (e.g. Hönninger *et al.*, 2004b; Carlson *et al.*, 2010; Galle *et al.*, 2010).

Light converges within the telescope at the focal point where the optical fiber connector is located and is transmitted through an optical fiber (Fiber Tech Optica, quarz, 6 m long, $\varnothing = 0.6$ mm), which exits the box just across the telescope opening, into the acquisition/control unit. The current optical configuration allows us to have a theoretical FOV of 0.31°.

The entire scanner enclosure can be rotated so that the telescope can point at different elevation angles. This is accomplished by a stepper motor (Oriental Motors, PK266-02A) which is installed at the center of the scanning enclosure with the rotation axis looking outward (Fig. 1b). The axis of the motor is fastened to an outer plate that can be fixed to the vertical pole of a tripod, a wall, etc., allowing for the scanner to rotate in a range between -90° and 90° with respect to the zenith position (0°). The motor can make movements of 0.1° and a switch installed at one corner of the scanning box with a stopper fixed to the outer plate, is used as a reference to indicate the start position of each scan.

We designed a control board (Fig. 1c), which consists of a microcontroller (AVR architecture) that obtains data from the temperature sensor (Maxim 18B20, accuracy ± 0.5 °C) inside the scanner, the optical switch of the shutter and the external switch for the scanner's position. It receives and sends information to the computer, within the acquisition/control unit, through a connection cable. It contains

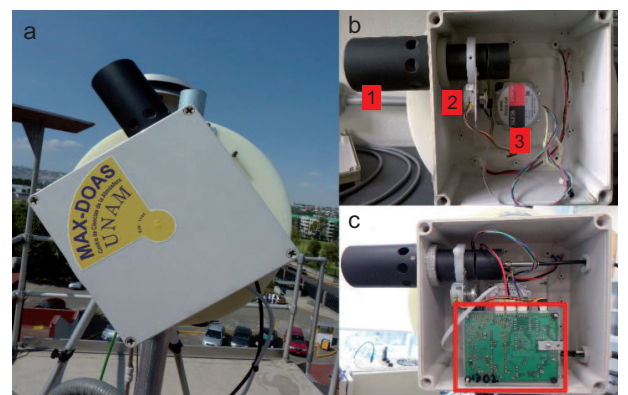


Fig. 1. (a) The scanner in operation. (b) Interior view of the scanner: (1) telescope with outer protective cylinder, (2) the motorized shutter, and (3) stepper motor for rotating the complete scanning unit. (c) The control board (marked with a red frame), which is used to control the stepper motors, is installed and ready for operation.

two motor drivers for controlling both motors, one for the shutter and the other for the scanner position. A dual axis accelerometer (Analog Devices, accuracy $\pm 0.1^\circ$) has been incorporated to the control board to determine, with previous calibration, the relative orientation of the telescope in each predetermined measurement position with respect to the zenith.

2.1.2 Acquisition and control unit

The acquisition and control unit is a resistant metallic housing ($400 \times 400 \times 200$ mm) which is typically installed indoors on the wall not too far from the scanner. It receives the light collected by the scanner, sends it to the spectrometer, controls and reads the motors and sensors, and records the information in a computer.

The small grating spectrometer (Ocean Optics, USB2000+) receives the light from the optical fiber. It has a crossed asymmetric Czerny-Turner configuration, uses a Charge-Coupled Device (CCD) detector array (Sony ILX511B) of 2048 pixels with an integration time adjustable between 1 ms to 65 s. This spectrometer, which has been used successfully by Galle *et al.* (2002), Hönniger *et al.* (2004b), Sinreich *et al.* (2005), and Johansson *et al.* (2009) in similar applications, was customized to operate at a spectral resolution of 0.69 nm full width at half maximum (FWHM); it has a grating with a groove density of 1800 lines/mm, a slit of 50 μm wide \times 1 mm high, an holographic UV blaze wavelength, and wavelength range of 286 to 510 nm.

It is important to have the spectrometer temperature-stabilized because the dark current, electronic

offset and the wavelength/pixel ratio of the detector are sensitive to temperature changes, which could also modify the optical properties of the spectrometer like the alignment and the line shape (Carlson *et al.*, 2010; Coburn *et al.*, 2011). We have therefore implemented an accurate temperature controller by attaching a Peltier cell (Multicomp) and three temperature sensors (Maxim 18B20, accuracy $\pm 0.5^\circ\text{C}$) to the spectrometer, and wrapped it in a Styrofoam box. As it can be seen in Figure 2b, the spectrometer was placed within a ventilated aluminum enclosure, which together with a heatsink ($150 \times 60 \times 20$ mm) at the warm side of the Peltier module allowed us to stabilize the temperature of the spectrometer at 20°C with a $\pm 0.5^\circ\text{C}$ precision. A fan (24 VDC, 0.1 A) extracts the hot air generated by the heatsink out of the box.

The control board in Figure 2b was designed to read data from the temperature sensors attached to the spectrometer, the Peltier cell and the heatsink, to regulate the current applied to the Peltier and to decide when the fan should be turned on. A power supply (24 VDC and 10A) is used to operate the control boards and power the stepper motors. The microcontroller AVR (8-bit) in the control board receives and sends information to the computer through an RS-232 port.

A laptop computer (Dell, Latitude 2021) with 3 USB ports, Ethernet and Linux operating system was fixed to the door of the acquisition/control unit. It runs a custom written program (C++, Qt platform) for controlling the hardware. A script running within this program is used to define the mea-

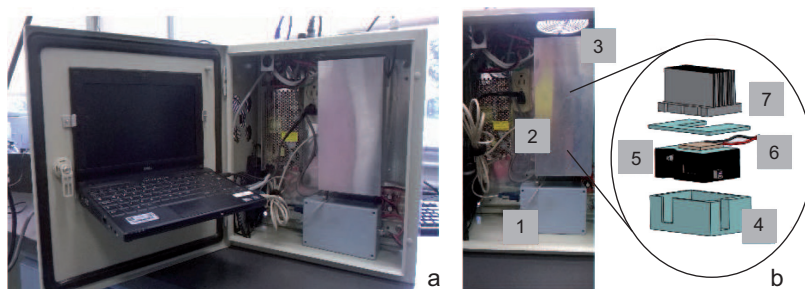


Fig. 2. (a) Acquisition and control unit, consisting of the computer, the cooling system and the spectrometer (better appreciated in the right panel). (b) The cooling system of the spectrometer is composed of: (1) a temperature control board, (2) an aluminum enclosure, (3) a fan, (4) a styrofoam box around the (5) spectrometer, which has a (6) Peltier cooling/heating module and a (7) heatsink attached on top of it (items 4-7 are located inside the aluminium enclosure).

surement sequence, spectrometer temperature and dark offset acquisition. The sequence includes two zenith measurements, one serving as the reference spectrum and one with closed shutter serving for the dark offset corrections. All the spectra and related information are stored in the computer for further processing. The computer has an internet port and the instrument can therefore be accessed remotely to download data and monitor its operation.

2.2 Measurement characteristics

2.2.1 Instrument operation

Once initialized, the instrument will continuously measure sequences and the times of the day to start and end operation can be set to avoid night records. We typically operate the instrument 12 h a day, beginning at 7:00 and finishing at 19:00 LT. In each scan, the scanner moves to the start position indicated by a stopper switch, moves to the zenith position (0°) taking a spectrum which is saved as reference, then moves to the position -90° with respect to the zenith and performs a cycle of measurements at the specified angles. In each position a maximum of 200 acquisitions are averaged to reduce the noise of the recorded spectra. When the scan is completed, the shutter is closed and a dark offset is recorded. The offset, however, is found to have a variability which is typically smaller than 3% thanks to a $\pm 0.3^\circ\text{C}$ stabilization of temperature, which is kept throughout the day.

For the results presented in this work, dark spectra are not used in the analysis. However, dark spectra measured after each scan will be considered in the analysis of VCD's (in a forthcoming paper).

In each cycle 36 spectra are recorded at different elevation angles, as well as one reference spectrum and one dark spectrum, taking less than 5 min to be completed. Although the duration of each cycle can vary, an average of 150 cycles is recorded per day. Figure 3 shows a drawing of (a) the elevation angles and (b) an example of the measured spectra within a sequence. The integration time is adjusted for each cycle by the intensity in the reference spectrum. It is also shown in the figure how the orientation of the scanner is defined by an azimuth angle with respect to the north.

2.2.2 Network sites

Four MAX-DOAS instruments were constructed and deployed in the metropolitan area of Mexico City. The locations of these stations are shown in the map on Figure 4, which are overlaid on average NO_2 column densities from the OMI satellite product (Rivera *et al.*, 2013). The underlying map produced with Cartopy (Met Office, 2015) uses map tiles from Open Street Map (OSM) Contributors[©] (<https://www.openstreetmap.org>). All instruments require internet services, electricity and safeguarding for continued monitoring, for this reason the instruments are located in four RAMA air quality stations. These stations measure continuous ground surface NO_2 , fine particulate matter ($\text{PM}_{2.5}$) and other parameters, which are of great value for further analysis of the retrieved column densities.

A summary of the station characteristics including their geographical location, altitude and telescope's azimuth angle (TAA) is included in Table I. A brief description of the stations is provided below.

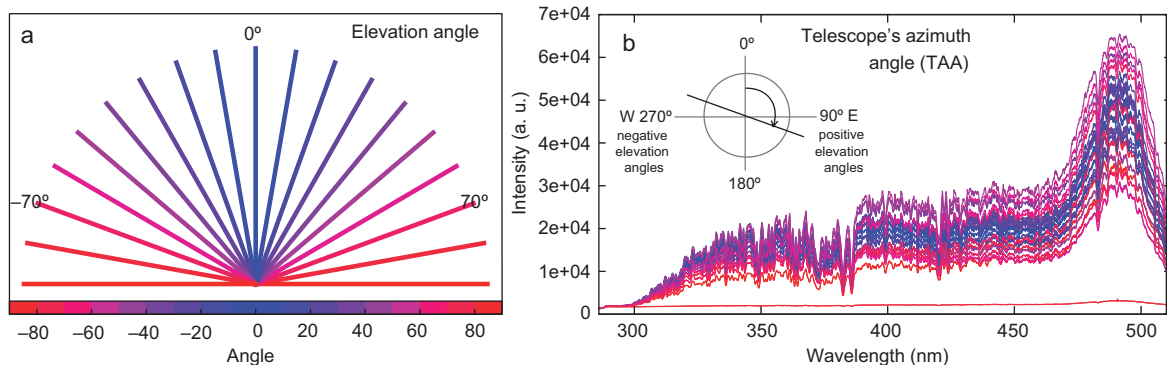


Fig. 3. (a) Sketch of how the scanner orientation is defined by a fixed telescope azimuth angle (TAA) with respect to the geographic coordinates and the pattern of 36 positions of the telescope's elevation angles at which measurements are performed with respect to the zenith position. (b) Example of measured spectra of a blue sky with a blue-to-red scale corresponding to increasing zenith angles.

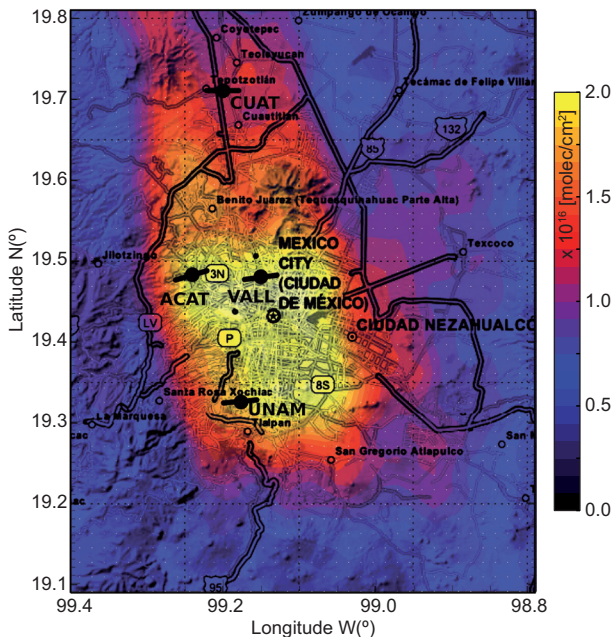


Fig. 4. Map of the Mexico City Metropolitan Area (MCMA) with the average horizontal distribution of NO_2 (in molecules/cm 2) from satellite measurements according to Rivera *et al.* (2013). Black circles with bars indicate the location and corresponding scanning orientations (TAA) of the MAX-DOAS instruments.

Table I. Sites where MAX-DOAS instruments have been installed within the Mexico City Metropolitan Area.

Sites	Latitude	Longitude	Altitude (masl)	TAA
UNAM	19.326	-99.176	2280	85°
ACAT	19.482	-99.243	2299	73°
CUAT	19.722	-99.198	2263	90°
VALL	19.483	-99.147	2255	83°

TAA: Telescope's azimuth angle.

UNAM. This station is located south of the city in our university campus, specifically on the rooftop of the Centro de Ciencias de la Atmósfera. The building has a measurement platform with sophisticated instrumentation which is part of the Red Universitaria de Observatorios Atmosféricos (University Network of Atmospheric Observatories, RUOA [www.ruoa.unam.mx]). The area towards the west is mostly residential and the ecological reserve of Pedregal de San Ángel can be found to the southwest; in contrast, the east and north directions of the station are highly urbanized.

ACAT. The Acatlán station is located in the north-western part of the city in a highly urbanized area with buildings surrounded by two parks, one of them to the south and the other to the north. The station is hosted by the campus of UNAM's Facultad de Estudios Superiores (School of Graduate Studies). The region is highly urbanized and at 1 km distance towards the east there is a principal road with heavy vehicular load (FIMEVIC, 2001). The Naucalpan industrial park is less than 4 km away towards the southeast of the station.

CUAT. The instrument at Cuautitlán is located inside an ecological park named Xochitla, in the far north of the city. This area has different points of interest; 1 km to the southwest of the station is the state highway with heavy transport use of factory products, and to the south there is an industrial park with different factories. This site should track pollution transport events to and from the city as has been described by Jazcilevich *et al.* (2003).

VALL. This station is located close to the downtown area in the Vallejo district. This is an industrial and highly urbanized area with a huge quantity of motor vehicles. This station is hosted by the operational office of the RAMA network and has therefore a large amount of instrumentation for atmospheric monitoring.

3. Spectral analysis

Spectra were evaluated using the QDOAS (v. 2.105) software (Danckert *et al.*, 2013). For NO_2 (shown in Fig. 5a) the retrieval was conducted in the 405 to 465 nm wavelength window. Differential cross-sections of NO_2 at 298 K (Vandaele *et al.*, 1998), O_3 at 221 K and 241 K (Burrows *et al.*, 1999), oxygen dimer O_4 (Hermans *et al.*, 1999), and a Ring spectrum generated at 273 K from a high resolution Kurucz file using the QDOAS software (Danckert *et al.*, 2013), were included in the analysis.

For HCHO the retrieval was conducted in the 335 to 357 nm wavelength window. Differential cross-sections of HCHO (Meller and Moortgat, 2000), BrO (Wilmouth *et al.*, 1999), NO_2 (Vandaele *et al.*, 1998), O_3 at 221 K and 241 K (Burrows *et al.*, 1999), oxygen dimer O_4 (Hermans *et al.*, 1999), and the previous Ring spectrum were also used for this analysis.

The high resolution spectra were convolved with a slit function of the spectrometer measured with a low

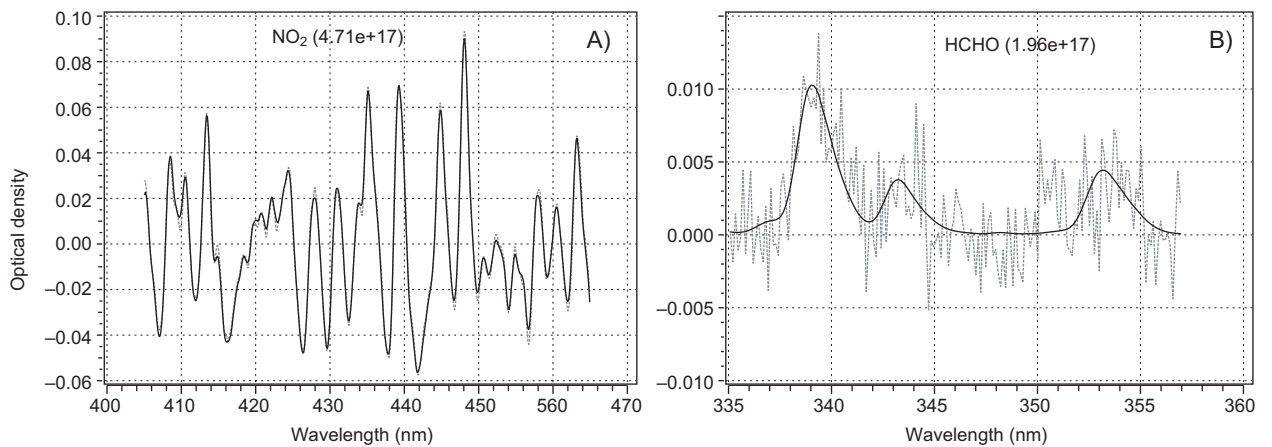


Fig. 5. Retrieval windows of (a) NO_2 and (b) HCHO from spectra measured on December 17, 2013 at 12:06 and February 1, 2013 at 10:54 LT, respectively. The black lines are the fitted spectra and the dotted gray lines the measured spectra.

pressure Hg lamp. Typical retrieval fits are shown in Figure 5. For this example, the retrieved NO_2 SCD was 4.71×10^{17} molecules/cm² with a fitting error of 2.43×10^{15} . For HCHO , the retrieved SCD was 1.96×10^{17} molec/cm² with an error of 2.31×10^{16} . The corresponding residuals were of the order of 10^{-3} RMS, as expected for compact DOAS systems.

4. Results

We present the results from measurements recorded at the UNAM station in the period from January 2013 to November 2014. Only SCDs of NO_2 and HCHO retrieved at angles of 70° and -70° are presented here, chosen to enhance sensitivity through longer optical paths and to ensure that the measurements had no interference by any object surrounding the observation site. The results from these two viewing orientations are shown independently in order to identify differences when viewing east and west, respectively.

All measurements were filtered to ensure a good fit from the QDOAS retrieval. The elevation angle for the reference spectrum should be close to 0° , so a variation of this angle should not exceed $\pm 1.2^\circ$. During the period from July 2013 to September 2013, the instrument at UNAM station had problems with the tuning of the elevation angle for the reference spectrum. Therefore, instead of the original reference spectrum, a measurement from the scan with an elevation angle in the range of $\pm 5^\circ$ was chosen as a replacement for the reference spectrum. All the data is treated and presented in a fixed local time corresponding to UT-06, avoiding summer time corrections. After filtering the data, 373 days of

measurements with 55 950 individual spectra are considered in this analysis.

4.1 NO_2

Figure 6 shows the average diurnal cycles (solid blue lines) from the NO_2 differential slant columns (at $\pm 70^\circ$ zenith angles) measured during the entire period towards the east (circles) and west (triangles) sides of the UNAM station. These curves peak at around 11:00–12:00 LT, which is consistent to what was observed by Rivera *et al.* (2013) during 2010–2011 with zenith scattered DOAS measurements, and also to the behavior reported in the emission inventory (SEDEMA, 2013).

To complement the analysis, surface NO_2 concentrations measured at two RAMA stations located towards the east (UAX, 110° , 8.2 km) and towards the west (PED, 266° , 2.9 km) were compiled and averaged. The dashed lines in Figure 6 are the average surface concentrations of NO_2 in ppb measured at these two RAMA stations, respectively. The surface concentrations (black) peak at least an hour earlier than the columns (gray) because the growth of the mixing layer during the late morning causes the concentrations at the surface to be diluted.

Due to the difference in methodologies and units, a direct comparison of surface and column amounts is not possible, however, in both cases a higher NO_2 is observed west of the UNAM station (triangles) than towards the east (circles). A simple explanation for this phenomenon is given by studies like that of Jazcilevich *et al.* (2003), reporting a general wind pattern towards the southwest corner of the MCMA transporting pollution predominately in this direction

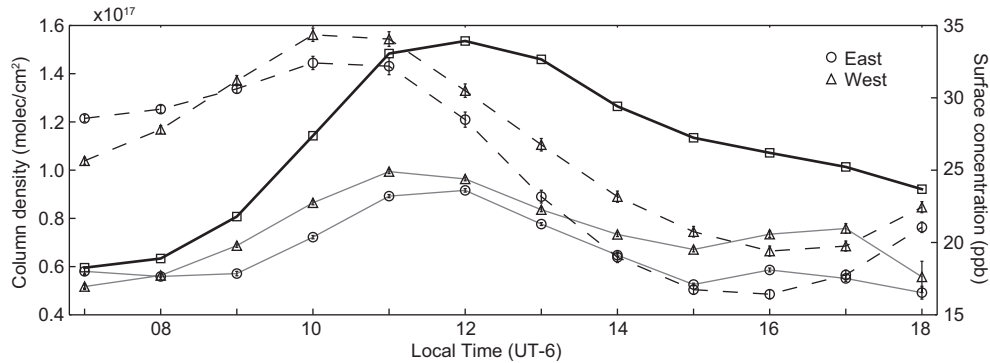


Fig. 6. Average diurnal variability of NO_2 over the UNAM site for the period between January 2013 and November 2014. The gray lines represent the differential slant columns measured at $\pm 70^\circ$ towards the east (circles) and west (triangles). The diurnal cycles of the average surface concentrations measured at two locations located east and west of the station are shown as dashed lines with circles and triangles, respectively. The black line represents the reconstructed slant column based on surface concentrations and the heights of the mixing layer measured at UNAM.

and presenting the slightly larger values of NO_2 seen in Figure 6. In average, NO_2 in PED starts lower and grows larger than in UAX after 9 h. This is also seen in the east-west slant column measurements and could be characteristic of a photochemically produced NO_2 from fresh emissions, which are released in larger amounts in the eastern and northern parts of the observation site.

A vertical column, in molecules/cm², was estimated by scaling the surface concentration (average of UAX and PED) with the height of the mixing layer and assuming a homogeneous distribution of NO_2 throughout the layer. The MLH is available at the UNAM station from backscattering measurements of pulsed laser light performed by a commercial ceilometer (Vaisala, model CL31), which is operated continuously at this site. It is important to say that for the sake of comparison with the SCDs measured with the MAX-DOAS instrument, that reconstructed vertical columns were multiplied by the geometrical factor of 2.9, obtained from $1/\cos 70^\circ$. The magenta line in Figure 6 represents thus the slant column of NO_2 reconstructed from surface concentrations and measured MLH's. As one would expect by comparing similar quantities, the slant columns measured with the MAX-DOAS instrument and the reconstructed column peak at approximately the same time.

There are differences, however, in both the form and magnitude of the diurnal cycles from the

reconstructed (magenta) and measured (blue) slant column densities. Inhomogeneity in the vertical distribution of the gas from the presence of inversion and residual layers at specific times may explain some of the differences observed, which has to some extent been documented specifically for the MCMA by several authors (Fast and Zhong, 1998; Lezama *et al.*, 2002; Shaw *et al.*, 2007; Melamed *et al.*, 2009; Stremme *et al.*, 2009). To account for the significant discrepancy of approximately 40% smaller columns of the measured slant columns with respect to the reconstructed ones from surface and MLH measurements, other aspects have also to be considered.

The calculation of the geometrical factor performed here assumes that scattering of photons takes place above the mixed layer and that all photons travel their way through the slant column to the instrument. However, there is scattering within the mixing layer of photons coming directly from the sun towards the line-of-sight of the instrument. Assuming single scattering, the absorption by a given gas would be less apparent, and an underestimation of the real column would be produced.

In this context it should also be mentioned that the difference between the diurnal cycle of the slant column towards east and west might partly be influenced by the evident differences in the relative angle of the sun and the corresponding viewing angles. This may cause that one particular direction may experience

more absorption above the scattering height than the other and that the phase function dependence contributes to the observed differences. This latter effect might be small for the spectral window above 400 nm used to retrieve NO_2 , but could be important for shorter wavelengths like those used in the analysis of HCHO.

4.2 HCHO

The average diurnal cycle of formaldehyde slant columns measured towards the east at a zenith angle of 70° (circles) and towards the west at -70° (triangles) from the UNAM station is presented in Figure 7. A large difference between the two observation directions is observed. In the mornings, a strong HCHO peak can be detected towards the east which is not seen when pointing west. This peak at 8:00 LT is consistent to what was measured by Grutter *et al.* (2005) in downtown Mexico City, where maxima of near surface concentrations were reported to occur during the early morning.

It is known that in Mexico City a significant amount of HCHO is associated with primary emissions (García *et al.*, 2006). It is not surprising to find high values towards the east because in this direction a large population density, a number of avenues and thus heavy traffic can be found. West of UNAM is characterized to have areas with vegetation, low urbanization and low emissions. Typical meteorological conditions in the MCMA comprise calm winds until about noon and then ventilation picks up and blows the pollution, frequently towards

the southwest (Jazcilevich *et al.*, 2003). This could explain the cross-over between the east and west curves in Figure 7 showing a progressive growth HCHO concentration from more aged masses to the west of the observation site.

5. Conclusions

In this article we have presented the design, construction and implementation of an instrument based on the MAX-DOAS technique. Four of these instruments, which now constitute a new network, have been installed and are operating in strategic locations within the MCMA. We have focused on describing the technical characteristics of both the scanning and acquisition units, and demonstrating their ability to detect NO_2 and HCHO in the atmosphere, which are key photochemical pollutants.

It is demonstrated in this work that the instruments are capable of producing valuable information from the diurnal variability of the measured slant columns of these gases. Filtered data from a period spanning almost two years are used in this analysis and compared to the reconstructed column amounts from measured surface concentrations and the heights of the mixing layer. Interesting features become apparent which can be related to the location of these particular sites within the city and the meteorological patterns associating the transport of pollutants. The results and discussion presented, however, also suggest the need to (1) incorporate the radiative transfer into the analysis and (2) include the data from instruments at other locations.

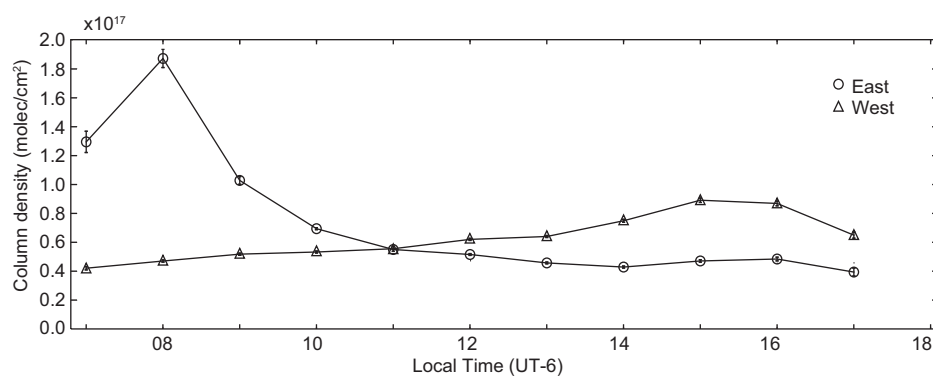


Fig. 7. Average diurnal variability of HCHO differential slant column (measured at $\pm 70^\circ$) over the UNAM site for the period between January 2013 and November 2014. The curve with circles represents the measurement towards the east and that with the triangles points west from the observation site.

There are many limitations of not taking advantage of the full multi-axis capability of these instruments and we have therefore developed a computational code based on a radiative transfer model and an inversion algorithm to gain information on the vertical distribution of the gases. This work is in preparation and will be presented elsewhere.

Future studies using all four sites will make it possible to understand the relationship between these chemical species and different environments, emission characteristics and meteorological patterns within the metropolitan area. The VCDs which will be obtained from these measurements have the potential to improve the air quality models currently deployed in the region for evaluating mitigation scenarios, for example, and to validate satellite products which are increasingly being used to acquire more information on the spatial distribution of the pollution in several parts of the world.

Acknowledgments

This project was funded by UNAM-DGAPA (IN109914) and by SEDEMA from the Gobierno del Distrito Federal, which are also thanked for making the air quality data available. J. Arellano would like to acknowledge CONACYT for the stipend which supported his Ph.D. work. Special thanks to A. Rodríguez from the mechanical workshop of the Centro de Ciencias de la Atmósfera for helping in the construction of the instruments. Thomas Danckaert, Caroline Fayt and Michel van Roozendael are thanked for making QDOAS available for the analysis.

References

Burrows J. P., A. Richter, A. Dehn, B. Deters, S. Himmelmann, S. Voigt and J. Orphal, 1999. Atmospheric remote sensing reference data from GOME-2. temperature dependent absorption cross sections of O₃ in the 231-794 nm range. *J. Quant. Spectrosc. Ra.* **61**, 509-517.

Carlson D., D. Donohoue, U. Platt and W. R. Simpson, 2010. A low power automated MAX-DOAS instrument for the Arctic and other remote unmanned locations. *Atmos. Meas. Tech.* **3**, 429-439.

Coburn S., B. Dix, R. Sinreich and R. Volkamer, 2011. The CU ground MAX-DOAS instrument: characterization of RMS noise limitations and first measurements near Pensacola, FL of BrO, IO, and CHOCHO. *Atmos. Meas. Tech.* **4**, 2421-2439.

Danckaert T., C. Fayt, M. Van Roozendael, I. De Smedt, V. Letocart, A. Merlaud and G. Pinardi, 2013. QDOAS Software user manual. Belgian Institute for Space Aeronomy, Uccle, Belgium, 117 pp.

Fast J. D. and S. Zhong, 1998. Meteorological factors associated with inhomogeneous ozone concentrations within the Mexico City basin. *J. Geophys. Res.* **103**, 18927-18946, doi:10.1029/98JD01725.

FIMEVIC 2001. Problemas de Movilidad en la Ciudad de Mexico. Fideicomiso para el Mejoramiento de las Vias de Comunicacion del DF. Available in: <http://www.fimevic.df.gob.mx/problemas/1diagnostico.htm>.

Galle B., C. Oppenheimer, A. Geyer, A. J. S. McGonigle, M. Edmonds and L. Horrocks, 2002. A miniaturised ultraviolet spectrometer for remote sensing of SO₂ fluxes: a new tool for volcano surveillance. *J. Volcanol. Geoth. Res.* **119**, 241-254.

Galle B., M. Johansson, C. Rivera, Y. Zhang, M. Kihlman, C. Kern, T. Lehmann, U. Platt, S. Arellano and S. Hidalgo, 2010. Network for Observation of Volcanic and Atmospheric Change (NOVAC). A global network for volcanic gas monitoring: Network layout and instrument description. *J. Geophys. Res. Atmos.* **115**, doi:10.1029/2009JD011823.

García A. R., R. Volkamer, L. T. Molina, M. J. Molina, J. Samuelson, J. Mellqvist, B. Galle, S. C. Herndon and C. E. Kolb, 2006. Separation of emitted and photochemical formaldehyde in Mexico City using a statistical analysis and a new pair of gas-phase tracers. *Atmos. Chem. Phys.* **6**, 4545-4557.

Grutter M., E. Flores, G. Andraca-Ayala and A. Báez, 2005. Formaldehyde levels in downtown Mexico City during 2003. *Atmos. Environ.* **39**, 1027-1034.

Hendrick F., J.-F. Miiller, K. Clemer, P. Wang, M. De Maziere, C. Fayt, C. Gielen, C. Hermans, J. Z. Ma, G. Pinardi, T. Stavrakou, T. Vlemmix, and M. Van Roozendael, 2014. Four years of ground-based MAX-DOAS observations of HONO and NO₂ in the Beijing area. *Atmos. Chem. Phys.* **14**, 765-781.

Hermans, C. A. C. Vandaele, M. Carleer, S. Fally, R. Colin, A. Jenouvrier, B. Coquart and M. F. M., 1999. Absorption cross-sections of atmospheric constituents: NO₂, O₃, and H₂O. *Environ. Sci. Pollut. R.* **6**, 151-158.

Hönninger G., N. Bobrowski, E. R. Palenque, R. Torrez and U. Platt, 2004a. Reactive bromine and sulfur emissions at salar de Uyuni, Bolivia. *Geophys. Res. Lett.* **31**, doi:10.1029/2003GL018818.

Hönniger G., C. von Friedeburg and U. Platt, 2004b. Multi Axis Differential Optical Absorption Spectroscopy (MAX-DOAS). *Atmos. Chem. Phys.* **4**, 231-254.

Jazcilevich, A. D., A. R. García and L. G. Ruiz-Suárez, 2003. A study of air flow patterns affecting pollutant concentrations in the Central Region of Mexico. *Atmos. Environ.* **37**, 183-193.

Johansson M., C. Rivera, B. de Foy, W. Lei, J. Song, Y. Zhang, B. Galle and L. Molina, 2009. Mobile mini-DOAS measurement of the outflow of NO₂ and HCHO from Mexico City. *Atmos. Chem. Phys.* **9**, 5647-5653.

Lezama J., R. Favela, L. Galindo, M. Ibarrarán, S. Sánchez, L. Molina, M. Molina, S. Connors and A. Bremauntz, 2002. Forces driving pollutant emissions in the MCMA. In: *Air Quality in the Mexico Megacity* (L. Molina and M. Molina, Eds.), Springer, Netherlands, pp. 61-104 (Alliance for Global Sustainability Bookseries, 2).

Melamed M. L., R. Basaldud, R. Steinbrecher, S. Emeis, L. G. Ruiz-Suárez and M. Grutter, 2009. Detection of pollution transport events southeast of Mexico City using ground-based visible spectroscopy measurements of nitrogen dioxide. *Atmos. Chem. Phys.* **9**, 4827-4840.

Meller R. and G. K. Moortgat, 2000. Temperature dependence of the absorption cross sections of formaldehyde between 223 K and 323 K in the wavelength range 225-375 nm. *J. Geophys. Res.* **105**, 7089-7101.

Met Office, 2010-2015. Cartopy: a cartographic python library with a matplotlib interface. Exeter, Devon. Available at: <http://scitools.org.uk/cartopy>.

Platt U. and J. Stutz, 2008. Differential Optical Absorption Spectroscopy: Principles and applications. Springer, Berlin, 598 pp. (Physics of Earth and Space Environments).

Rivera C., W. Stremme and M. Grutter, 2013. Nitrogen dioxide DOAS measurements from ground and space: Comparison of zenith scattered sunlight ground-based measurements and OMI data in Central Mexico. *Atmosfera* **26**, 401-414.

SEDEMA 2013. Inventario de emisiones contaminantes y de efecto invernadero 2012. Zona Metropolitana del Valle de Mexico. Secretaria de Medio Ambiente. Gobierno del Distrito Federal. Available in: <http://www.aire.df.gob.mx>.

Shaw W. J., M. S. Pekour, R. L. Coulter, T. J. Martin and J. T. Walters, 2007. The daytime mixing layer observed by radiosonde, profiler, and lidar during MILAGRO. *Atmos. Chem. Phys. Discuss.* **7**, 15025-15065.

Sinreich R., U. Frie, W. Wagner and U. Platt, 2005. Multi Axis Differential Optical Absorption Spectroscopy (MAX-DOAS) of gas and aerosol distributions. *Faraday Discuss.* **130**, 153-164.

Stremme W., I. Ortega and M. Grutter, 2009. Using ground-based solar and lunar infrared spectroscopy to study the diurnal trend of carbon monoxide in the Mexico City boundary layer. *Atmos. Chem. Phys.* **9**, 8061-8078.

Stutz J., B. Aliche and A. Neftel, 2002. Nitrous acid formation in the urban atmosphere: Gradient measurements of NO₂ and HONO over grass in Milan, Italy. *J. Geophys. Res. Atmos.* **107**, doi:10.1029/2001JD000390.

Vandaele A. C., C. Hermans, P. C. Simon, M. Carleer, R. Colin, S. Fally, M. F. Merienne, A. Jenouvrier and B. Coquart, 1998. Measurements of the NO₂ absorption cross-section from 42 000 cm⁻¹ to 10 000 cm⁻¹ (238-1000 nm) at 220 K and 294 K. *J. Quant. Spectrosc. Ra.* **59**, 171-184.

WHO 2014. Burden of disease from ambient air pollution for 2012. World Health Organization. Geneva. Available in: <http://www.who.int/phe/healthtopics/outdoorair/databases/en/>.

Wilmouth D. M., T. F. Hanisco, N. M. Donahue and J. G. Anderson, 1999. Fourier transform ultraviolet spectroscopy of the a2n3/2- x2n3/2 transition of BrO. *J. Phys. Chem. A* **103**, 89358945.

WPR 2014. World Population Report. Available in: <http://worldpopulationreview.com/world-cities/mexico-city-population/>.